JACS
JOURNAL OF THE AMERICAN CHEMICAL SOCIETY
Article
pubs.acs.org/JACS

Stern Layer Formation Induced by Hydrophobic Interactions: A Molecular Level Study

Rüdiger Scheu,[†] Yixing Chen,[†] Mireia Subinya,[‡] and Sylvie Roke*,[†]

[†]Laboratory for fundamental BioPhotonics (LBP), Institute of Bioengineering (IBI), School of Engineering, École Polytechnique Fédérale de Lausanne (EPFL), 1015 Lausanne, Switzerland

[‡]Institute of Physical Chemistry, University of Stuttgart, 70569 Stuttgart, Germany

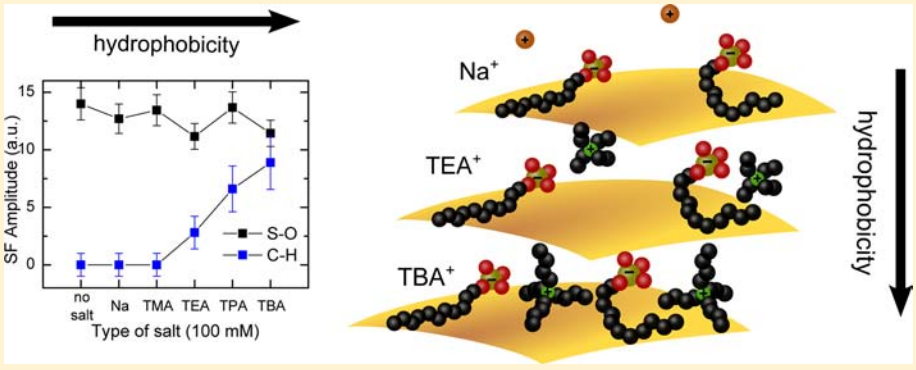

ABSTRACT: The molecular ionic surface structure and charge of the electric double layer around a nanodroplet and its structural change induced by hydrophobic effects are measured using vibrational coherent surface scattering spectroscopy, second harmonic scattering, and electrokinetic mobility measurements. Tetraalkylammonium chloride salts were added to negatively charged nanoscopic oil droplets in water. When we vary the alkyl chain length of the cation from CH_3 to C_4H_{10}, both the size of the cation and its hydrophobic interaction are increased. We find that tetramethylammonium ions change the electrokinetic potential and the water structure but do not detectably adsorb to the interface. Tetrapropylammonium and tetrabutylammonium ions clearly adsorb to the interface. The corresponding (Stern) layer appears to be a mixed monolayer of anions and cations. An estimate of the amount of cations in the Stern layer is also made.

INTRODUCTION

Roughly 60% of the human body consists of water, which is continuously in contact with biochemical constituents and dissolved ions. The subnanometer thick interfacial contact region of water with macromolecules or biomembranes typically comprises hydrophobic and (charged) hydrophilic parts. Specific ion effects[1−3] and hydrophobic effects,[4,5] which are closely linked (especially in a biochemical context),[6,7] greatly influence the structure and properties of the interface and the adjacent electric double layer,[8] and thus affect membrane formation, self-assembly, and stability.[9−13] The interplay of specific ion effects and hydrophobicity[6,7,12,14,15] is also relevant for the adsorption,[16−20] aggregation[20,21] and folding/unfolding[22] of proteins and peptides. Here, the intricate interplay of specific effects from the ionic groups on amino acids, the entropic interactions that result from the collective hydrophobicity and related shape changes, and the chemically specific interaction with the surface are all important factors that determine the adsorption of proteins. Specific ion effects have been studied in aqueous solutions (see, e.g., refs 10 and 23 and references therein), and in the context of interfaces.[3,6,11,14,24]

Recent theoretical[14,25−27] and experimental studies[28−41] have shown that understanding of specific ion effects is complicated because the solvation structure near the interface plays an important role.[42] Experimental studies have been performed with X-ray photolelectron spectroscopy of ions situated within several nanometers of the air/water interface (as determined by the penetration depth of the probe) of a liquid jet.[25] Second harmonic (SH) generation measurements of the surface potential of polystyrene particles and of emulsion droplets and liposomes[43,44] have been performed as well as resonant SH reflection measurements[34] and sum frequency generation measurements[35] of nitrate ions at the quartz/water interface. These studies showed that it is possible to measure the resonant response of the interfacial ions, and reported how this response is affected by different counterions. Moreover, sum frequency generation measurements demonstrated the strong influence of specific ion effects on the interfacial water structure at air/water interfaces,[28,29] hydrophilic/water interfaces,[30−32] and mixed hydrophobic−hydrophilic/water interfaces.[33,45] To our knowledge, a simultaneous measurement of the structure of

Received: October 7, 2013
Published: December 9, 2013

dx.doi.org/10.1021/ja4102858 | J. Am. Chem. Soc. 2013, 135, 19330−19335

all molecular actors as well as the electrokinetic properties of an interface has not been performed. Similarly, hydrophobic effects are determined by the hydration of solutes and the hydrophobic structure. For the hydration of hydrophobic solutes, the nanometer length scale is an important crossover point from molecular to microscopic behavior (refs 5, 46−51, and references therein). Molecular surface studies that specifically address the relationship between hydrophobicity and specific ion effects have not been performed either. To quantify the intricate balance of specific ion effects and hydrophobicity, such studies are necessary.

Here, we quantify specific ion effects at a charged hydrophobic interface with surface and charge specific techniques. We measure the surface structure of anions, cations, and water, and the electrokinetic potential of a negatively charged liquid hydrophobic/water interface in contact with a solution that contains tetraalkylammonium (TAA^+) ions. We tune the size and hydrophobicity of the cations in the solution by increasing the alkyl chain length of the TAA^+ cations from methyl, with a cationic diameter of <1 nm, to butyl with a cationic diameter of >1 nm. We find that tetramethylammonium (TMA^+) ions change the electrokinetic potential and the water structure but do not detectably adsorb onto the interface. Tetraethylammonium (TEA^+) ions adsorb weakly onto the interface. Stronger surface adsorption occurs for tetrapropylammonium (TPA^+) and tetrabutylammonium (TBA^+) ions. There is thus a strong possibility that a Stern layer is formed with TPA^+/TBA^+ and the surface adsorbed amphiphilic anions. In this layer, the cations and anions are likely organized in a mixed monolayer structure. First, we briefly motivate and introduce the methods and then describe our results, from which the molecular structure and charge of the layer is derived.

We use a solution of negatively charged (amphiphile-stabilized) nanoscopic liquid hexadecane droplets in an aqueous solution. Such a system mimics the multitude of charged hydrophobic/water interfaces in a biochemical environment, and captures the essential size range and charge density of objects present therein. With droplet sizes of ∼100 nm, it also contains an extremely large surface to volume ratio in a small sample volume (∼3000 cm^2/mL), which ensures an improved signal-to-noise ratio and reduced sensitivity to impurities compared to measurements on planar interfaces. It further allows for simultaneous charge and surface structure measurements.

Electrokinetic mobility measurements are used to measure the electrostatic potential of the surface region and to probe the amount of charge contained within the slip plane.[8] The surface structure of water can be tracked with second harmonic[52] scattering[53] (SHS), that occurs only in noncentrosymmetric regions and therefore probes anisotropically oriented water molecules, as induced by the interface and/or an electric field that may distort the otherwise isotropic distribution of water molecules in the bulk phase.[40,54−56]

The surface structure of anions and cations at the charged hydrophobic/water interface was measured with vibrational Sum Frequency Scattering (SFS), a vibrational coherent surface spectroscopy that measures the combined IR and Raman spectrum of molecules that can only give rise to signal in noncentrosymmetric environments such as interfaces.[57,58] As with SHS, the orientational correlations within the sample are probed. Since SFS is a resonant method, a specific cationic or anionic molecular species can be followed. Cations and anions that exhibit no dipole moment will not be affected in their orientational distribution by the static interfacial electric field (in contrast to the dipolar water molecules). The probing depth for adsorbates is therefore typically 1−3 molecular layers,[58] and is thus shorter than that of SHS. The SF intensity for each vibrational mode scales quadratically with its surface density, multiplied by the square of the average cosine of the tilt angle of the moieties' symmetry axis with the interface normal.[59,60] Vibrational modes associated with groups that lie in the surface plane are therefore not observed. In contrast to SF generation in reflection mode, for small droplets (radius <200 nm), the SF spectrum recorded in polarization combinations SSP and PPP does not change in spectral shape when a molecule changes its orientation.[61] Interfacial dodecylsulfate (DS^-) anions are tracked by probing the sulfate stretch (S−O) mode (∼1070 cm^{-1}) and the interfacial TAA^+ cations are tracked by probing the alkyl (C−H) vibrational response. For our SFS experiments, the estimated detection limit is ∼1 molecule/27 nm^2 droplet surface area (for ∼100 nm droplets in a 1−2 vol% droplet solution).[62] Selective deuteration of both the oil phase and DS^- ions allows us to selectively probe the cations, since C−D and C−H modes vibrate at different frequencies. The C−H stretch spectral region contains valuable information about the alkyl chain conformation and geometry. The amplitude ratio (d^+/r^+) of the symmetric methylene (d^+, at ∼2850 cm^{-1}) and the symmetric methyl (r^+, at ∼2874 cm^{-1}) stretch vibrational modes is a common indicator for the conformation of alkyl chains.[63−65] A value of $d^+/r^+ \ll 1$ is associated with a stretched alkyl chain, i.e., an all-trans conformation, whereas a value of $d^+/r^+ > 1$ indicates that gauche defects dominate the measured SF spectra. The combination of electrokinetic measurements, SHS and SFS thus allows us to retrieve a complete molecular level picture of how the increasing hydrophobicity of the counterions affects the interfacial structure of the nanoscopic oil droplet-water interface.

RESULTS

Figure 1 shows the electrokinetic zeta potential and the SHS intensity of hexadecane nanodroplets (∼100 nm radius) stabilized with 10 mM sodium dodecylsulfate (SDS) in pure D_2O, or aqueous solutions of 100 mM NaCl , TMACl, TEACl,

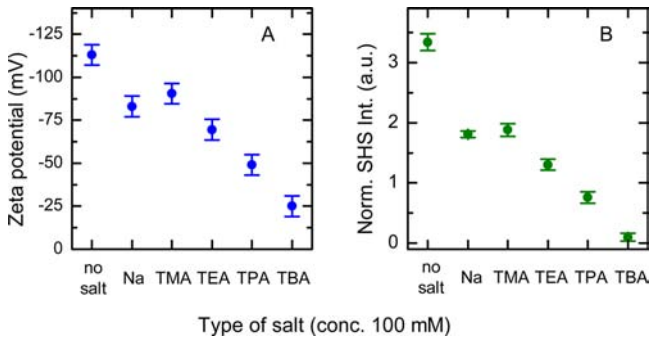

Figure 1. Electrokinetic potential and water structure. (A) Zeta potential of DS^--stabilized *n*-hexadecane nanodroplets in solutions without added salt, and with 100 mM of NaCl, TMACl, TEACl, TPACl and TBACl, respectively. (B) SHS signal of the same droplet samples, showing that the average orientational distribution of water molecules near the surface changes. SHS intensities were measured at a scattering angle of 35° with respect to the incoming beam and in PP polarization (i.e., all beams polarized in the scattering plane) and normalized as described in the text.

dx.doi.org/10.1021/ja4102858 | J. Am. Chem. Soc. 2013, 135, 19330−19335

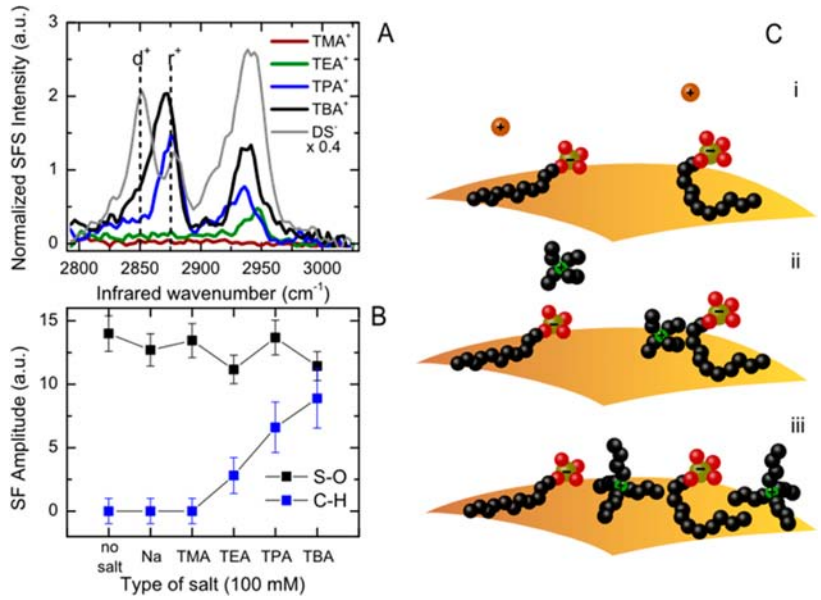

Figure 2. Surface structure of amphiphilic anions and cations. SFS spectra of hexadecane nanodroplets stabilized with 10 mM -SDS in pure D_2O, and in aqueous (D_2O) solutions of 100 mM of TMACl, TEACl, TPACl, and TBACl, respectively. The spectra are recorded in SSP polarization combination (i.e., the SFG and VIS beams are polarized perpendicular to the scattering plane, while the IR beam is polarized in the scattering plane). (A) SFS spectra taken in the C−H stretch region, displaying the relative amount of cations on the interface. The (scaled) spectrum of h-DS$^-$ ions on the droplet interface for a sample with 10 mM h-SDS in pure D_2O is also shown. No SF peaks are observed for the solution with 100 mM NaCl. (B) Integrated amplitudes of the C−H and S−O SF signals indicating the relative amount of TAA$^+$ cations and DS$^-$ anions on the surface. The charge density resulting from the adsorption of DS$^-$ ions is constant, while the cationic surface density increases with increasing alkyl chain length. (C) A possible illustration of the surface structure that agrees with the data. From top to bottom: surface with DS$^-$ and (i) Na$^+$, (ii) TEA$^+$, and (iii) TBA$^+$ ions.

TPACl, and TBACl, respectively. NaCl is neutral with respect to surface activity and is thus used as a reference.[66] It can be seen that the magnitude of the zeta potential decreases from the salt free solution to NaCl, and TMACl. The magnitude decreases approximately 20 mV per additional methylene group of the substituent chains, from −69 mV for TEACl to −25 mV for TBACl. Figure 1B displays the corresponding interfacial SHS signal (with beams polarized along the scattering plane, i.e., in PP polarization combination). The SH scattering of the aqueous solution (i.e., the hyper Rayleigh scattering from the water phase) was subtracted from the measured SHS signal. The obtained value is normalized to the hyper Rayleigh response of pure water as detailed in ref 67. The change in the SHS intensity is similar to the change in the magnitude of the zeta potential; it decreases when salt is added to the solution and further decreases with increasing ion size, i.e., increasing number of methylene groups in the substituent chains.

Figure 2 shows SFS spectra of hexadecane oil nanodroplets prepared with deuterated *d*-hexadecane, and 10 mM of deuterated SDS in pure D_2O, and aqueous solutions of 100 mM of TMACl, TEACl, TPACl, and TBACl, respectively. Figure 2A displays the SF signal of the C−H modes of only the TAA$^+$ ions that are adsorbed to the surface (since the oil and DS$^-$ ions were both deuterated and their resonance frequencies are hence shifted to lower frequencies). The gray line represents a reference DS$^-$ alkyl chain spectrum recorded from a solution with 10 mM of nondeuterated SDS without additional salts. Figure 2B displays the square root of the integrated intensities of the S−O response of the DS$^-$ anions (spectra not shown) and of the C−H response of the TAA$^+$ cations. It can be seen that the density of sulfate head groups of DS$^-$ ions on the interface is not changing with different dissolved cations, while the density of TAA$^+$ ions increases for longer alkyl chains; solutions with droplets and TMA$^+$ ions do not display any surface signal. For TEA$^+$ ions, weak features of probably the Fermi resonance (2941 cm^{-1}) are visible. However, clear spectral signatures of the symmetric (2874 cm^{-1}) and antisymmetric methyl stretch modes as well as the Fermi resonance appear in droplet solutions with TPA$^+$ and TBA$^+$ cations.

DISCUSSION

Size of Hydrophobic Chains. The absolute zeta potential values (Figure 1A) decrease gradually as larger and more hydrophobic cations are added to the solution. For Na$^+$ and TMA$^+$ cations, the zeta potential is approximately equal, with a magnitude 20 mV lower than for the salt-free solution. For these ionic solutions, the SHS signal decreases as well, which indicates that the interfacial water structure changes. For these ions, no SFS signal is detected from the interface (Figure 2A), which indicates that TMA$^+$ ions do not adsorb onto the surface. Given the estimated detection limit of 1 molecule per 27 nm^2 surface area,[62] we conclude that probably the majority of the TMA$^+$ ions reside in the aqueous phase close to the surface, where they change both the zeta potential and the orientational distribution of water molecules, but do not appear in the SFS spectra. The decrease of the zeta potential upon adding Na$^+$ and TMA$^+$ ions to the solution is likely caused by a compression of the double layer. Such a compression also changes the number of water molecules that are aligned by the electric field and thus reduces the SHS signal. With increasing size of the ions, the electrostatic potential inside the slip plane is reduced further as larger, more polarizable ions are closer to a hydrophobic surface.[27,68,69] For the solutions containing TEA$^+$, and to a larger degree for those containing TPA$^+$ and TBA$^+$, the

dx.doi.org/10.1021/ja4102858 | J. Am. Chem. Soc. 2013, 135, 19330−19335

SFS signal shows that the cations adsorb onto the negatively charged oil−water interface. This indicates that an adsorbed double (Stern) layer is formed with TBA^+ and TPA^+ ions, while TMA^+ and Na^+ ions appear to reside in the diffuse double layer (and not on the surface). Thus, surface adsorption is here observed when the hydrophobic domains increase their size above ∼1 nm. This particular size range of the cationic hydrophobic domains coincides with the size range for which hydrophobic solvation changes.[5,46−51] For TAA^+ ions, Raman hydration shell spectra showed that there is a nonlinear dependence on the number of dangling OH bonds and the exposed surface area of a solute.[70] This nonlinear dependence, which is interpreted as cooperative behavior, starts at an alkyl chain length of 3 carbon atoms per alkyl chain (i.e., for TPA^+ ions). In going from solute−solvent interactions[70] to interfacial adsorption as described here, there thus appears to be agreement with this work. Before estimating the surface charge densities, we first turn to the molecular conformation of the cations.

Interfacial Molecular Conformation of the Cations. The relative intensities of the symmetric methylene (d^+) and methyl (r^+) stretch modes are an indicator for the alkyl chain conformation. The SF spectra of the TPA^+ and TBA^+ ions are dominated by the methyl stretch mode, while the methylene stretch mode is nearly absent, i.e., $d^+/r^+ \ll 1$. For TPA^+ ions with an even number of CH_2 groups, the small contribution of the d^+ mode might be explained by an all-trans configuration of the four alkyl chains. In such a configuration, the polarization from the two methylene groups in each side chain interferes destructively as a consequence of local inversion symmetry. However, this configuration would not explain the nearly absent d^+ mode in the case of TBA^+ ions, which have an odd number of methylene groups in each side chain. A configuration that would explain the spectra of both TPA^+ and TBA^+ ions consists of one side chain pointing into the water phase and the three residual side chains aligned along the interface (as illustrated in Figure 2C). In this scenario, the methyl group that is pointing toward the water phase would mainly contribute to the spectral signature. The methylene groups will have their symmetry axis aligned with the surface plane, so that they do not contribute to the SFS signal. Although not definitive, this interpretation is in agreement with angle-resolved photoelectron spectroscopy measurements and molecular dynamics simulation studies of the air−water and air-formamide interface.[25,69,71] The TEA^+ ion may adopt a different conformation, but the low signal-to-noise ratio makes its spectrum difficult to interpret.

Surface Charge Density. Previous SFS measurements of DS^- ions on nanoscopic hexadecane droplets showed that the surface density of DS^- ions amounts to at most one ionic amphiphile of negative charge per 4.25 nm^2, which corresponds to a minimum surface spacing of ∼1−2 nm between neighboring ions.[72] The interfacial DS^- ions have a conformation that consists of predominantly parallel alkyl chains attached to a charged hydrated headgroup that remains entirely in the water phase.[73] Converting the surface density of DS^- ions to a surface charge density, assuming full ionization of the sulfate head groups, results in a maximum negative surface charge density of −0.037 C/m^2 (= −3.7 $\mu C/cm^2$). The intensity of the S−O stretch vibration, and consequently the interfacial density of the DS^- ions, varies little for all salt solutions (Figure 2B). This shows that the surface active TAA^+ ions do not compete with DS^- ions for empty surface sites.

By comparing the relative strength of the methyl stretch modes of DS^- and TAA^+ ions, we can make a rough estimate of the interfacial density of cations from the known interfacial density of DS^- ions. This computation should be treated with caution, as there are several complications in comparing the spectra, namely, (a) the droplets of the reference sample used for the DS^- reference spectra are not made in the same batch as the one shown in Figure 2, so that the droplet size distribution is slightly different, (b) the conformation and orientation of the CH_3 groups of the cations and DS^- anions are different. On the basis of our concluded alkyl chain conformation, mainly one methyl group per cation contributes to the signal. The TAA^+ methyl group is likely oriented more normal to the interface than the methyl group of the DS^- anion, which is predominantly oriented parallel to the interface,[73] and therefore contributes more to the signal. The charge density originating from cations absorbed onto the interface, as estimated by comparing the relative strengths of the methyl response, therefore represents an estimate of the maximum cation density. The resulting charge density from adsorbed TBA^+ ions is 0.85 × 3.7 $\mu C/cm^2$ = 3.1 $\mu C/cm^2$ and that from adsorbed TPA^+ ions is 0.72 × 3.7 $\mu C/cm^2$ = 2.6 $\mu C/cm^2$. These numbers agree well with the reduction in the magnitude of the zeta potential, as shown in Figure 1.

Stern Layer Structure. The electric double layer can contain adsorbed ions and diffusely bound ions that are free to move. A Stern layer is formed when the counterions are immediately adjacent or paired to surface charges. The SFS data shows that the surface charge density from anions is constant while the surface charge density from cations increases with increasing alkyl chain length of the cations' side chains. DS^- ions indeed form an adsorbed interfacial layer with TBA^+ and TPA^+ ions. These counterions could be paired (i.e., in immediate proximity) to the DS^- anions, or there could be water molecules in between. Furthermore, both ions could be in plane, or placed such that the DS^- ions are closer to the oil phase, with the TAA^+ ions further away, or opposite. From our data we find that the surface activity decreases in the order $TBA^+ > TPA^+ > TEA^+ > TMA^+$. Furthermore, the water orientational ordering decreases when more hydrophobic cations adsorb to the interface and partially neutralize the negative charge.

Ion pairs are formed most effectively, when charged groups are of similar size.[1] Because we observe most effective surface adsorption for TBA^+ ions, it is more likely that the alkyl chains of TBA^+ ions interact with the oil phase (rather than the ionic groups with each other). It is possible that there is water in between the DS^- ions and the counterions. Indeed, DS^- ions are well hydrated.[73] For TBA^+ ions there are more adsorbed counterions than for TPA^+ and TEA^+ ions, but the water orientional ordering is reduced. This excludes the formation of a capacitor-like film with DS^- ions closer to the surface and TPA^+/TBA^+ ions further away and water in between. The stronger electric field between the DS^- and TPA^+/TBA^+ ions or adjacent to the paired ions would align more water molecules and thus increase the SHS signal, which is not observed. With respect to the position of the ions and based on the above discussion, it is unlikely that TPA^+/TBA^+ ions will position themselves primarily in the water phase above the negative DS^- ions. Since we observed that dodecyltrimethyl ammonium ions perturb the oil phase of similar droplets,[74] it is more plausible that TBA^+ and TPA^+ ions form a mixed

dx.doi.org/10.1021/ja4102858 | J. Am. Chem. Soc. 2013, 135, 19330−19335

monolayer with DS^- ions or a structure in which the cations are closer or even somewhat inside the hydrophobic phase.

CONCLUSIONS

The electrokinetic potential and the molecular ionic and aqueous surface structure of a charged hydrophobic/water interface and its structural change as induced by hydrophobic effects are measured using vibrational coherent surface scattering spectroscopy, second harmonic scattering and electrokinetic mobility measurements. We find that the electrostatic potential and the interfacial orientational distribution of water molecules are strongly influenced and that starting from a hydrophobic chain length of ~1 nm the cations also adsorb on the interface. The interfacial structure that explains the data best is one where the anions and cations form a mixed monolayer or a structure in which the cations are closer or even somewhat inside the hydrophobic phase. Both structures will lead to an interface with less preferential orientational ordering of the water molecules and may have some resemblance to the ion and water structure around a zwitterionic phospholipid film.[33] A capacitor-like Stern layer with water aligned in between anions and hydrated cations can be excluded based on our measurements.

The interaction of ions with aqueous interfaces and the resulting electrostatic properties influences a wide range of biological, chemical, geological, and industrial processes. Our results show that the structure of the double layer changes quite dramatically when hydrophobic interactions are tuned and demonstrate that a hydrophobic domain size of ~1 nm is important for the interfacial organization of ions and water molecules.

MATERIALS AND METHODS

d-C_{16} (98% d, Cambridge Isotope), d-SDS (99% d, Cambridge Isotope), TMACl (99%, Fluka), TEACl (98%, Sigma-Aldrich), TPACl (98%, Sigma-Aldrich), TBACl (97%, Sigma-Aldrich) and D_2O (99%, Sigma-Aldrich) were used as received. Glassware was cleaned with a 3:7 H_2O_2:H_2SO_4-solution, after which it was thoroughly rinsed with ultrapure water (0.053 μS/cm,TKA).

Dispersions of oil droplets in water were prepared with 2 v/v % of deuterated hexadecane (*d*-C_{16}) in solutions of 20 mM of deuterated sodium dodecyl sulfate (*d*-SDS) in D_2O. The solutions were mixed for 1 min with a hand-held homogenizer (TH, OMNI International) and subsequently placed in an ultrasonic bath (35 kHz, 400 W, Bandelin) for 4 min. The resultant stock emulsion was then diluted with a solution of 200 mM of the respective tetraalkyl ammonium chloride in D_2O. The size distribution and the zeta potential of the droplets were measured with dynamic light scattering and laser Doppler electrophoresis (Zetasizer Nano ZS, Malvern).

Second Harmonic Scattering. Second harmonic scattering measurements were performed, as previously described in detail,[75] using 190 fs laser pulses centered at 1028 nm with a 200 kHz repetition rate. The polarized pulses were focused into a cylindrical glass sample cell (4.2 mm inner diameter). The scattered SH light was collimated with a plano-convex lens (f = 5 cm) and then sequentially passed through an iris to control the angular resolution and a bandpass filter. The filtered SH light was focused into a PMT by a plano-convex lens (f = 3 mm). The gate width of the PMT was 10 ns, the acquisition time was 1 s, and 40 acquisitions were averaged for each data point. A quarter-wave plate, a half-wave plate and a linear polarizer were used to control the polarization of the incoming fundamental beam. The polarization of the scattered light was analyzed with another polarizer. The SH signals were measured at a scattering angle of 35° with an angular resolution of ±1.75°.

Vibrational SFS Spectra. Vibrational SFS spectra were measured, as previously described in detail[61,76] using broadband infrared (IR) laser pulses centered at 2900 cm^{-1} (120 cm^{-1} FWHM bandwidth) and visible (VIS) pulses at 800 nm (12 cm^{-1} FWHM) at a repetition rate of 1 kHz. The focused laser beams were overlapped under an angle of 15° in a sample cuvette with a path length of 200 μm. At a scattering angle of 60°, the scattered SF light was collimated with a plano-convex lens (f = 15 mm, Thorlabs LA1540-B) and then passed through two short wave pass filters (third Millenium, 3RD770SP and Thorlabs FES750). The SF light was spectrally dispersed with a monochromator (Shamrock 303i, Andor Technologies) and detected with an intensified CCD camera (i-Star DH742, Andor Technologies) using a gate width of 8 ns. The acquisition time of a single spectrum was 300 s. A Glan-Taylor prism (Thorlabs, GT15-B), a half-wave plate plus a polarizer (Thorlabs, LPVIS) and two BaF_2 wire grid polarizers (Thorlabs, WP25H-B) were used to control the polarization of the SF, VIS and IR beams, respectively. All shown SFS spectra were normalized by the IR spectrum which was measured by SFG in reflection geometry from a z-cut quartz crystal.

Abbreviations. TAA, tetraalkyl ammonium; TMA, TEA, TPA, TBA, tetramethyl/ethyl/propyl/butyl ammonium; SDS, sodium dodecylsulfate, SFS, sum frequency scattering; SHS, second harmonic scattering; SSP, a polarization combination with an S polarized sum frequency beam, an S polarized visible beam and a P polarized IR beam, PP, a polarization combination with a P polarized second harmonic beam, and P polarized visible beams.

AUTHOR INFORMATION

Corresponding Author

sylvie.roke@epfl.ch

Notes

The authors declare no competing financial interest.

ACKNOWLEDGMENTS

This work is supported by the Julia Jacobi Foundation, the Swiss National Science Foundation (grant number 200021_140472), and the European Research Council (grant number 240556).

REFERENCES

(1) Kunz, W. *Specific Ion Effects*; World Scientific Publishing Company: Hackensack, NJ, 2009.
(2) Gurau, M. C.; Lim, S.-M.; Castellana, E. T.; Albertorio, F.; Kataoka, S.; Cremer, P. S. *J. Am. Chem. Soc.* **2004**, *126*, 10522−10523.
(3) Jungwirth, P.; Tobias, D. J. *Chem. Rev.* **2006**, *106*, 1259−1281.
(4) Blokzijl, W.; Engberts, J. B. F. N. *Angew. Chem., Int. Ed. Engl.* **1993**, *32*, 1545−1579.
(5) Chandler, D. *Nature* **2005**, *437*, 640−7.
(6) Lund, M.; Vacha, R.; Jungwirth, P. *Langmuir* **2008**, *24*, 3387−3391.
(7) Horinek, D.; Herz, A.; Vrbka, L.; Sedlmeier, F.; Mamatkulov, S. I.; Netz, R. R. *Chem. Phys. Lett.* **2009**, *479*, 173−183.
(8) Hunter, R. J. *Foundations of Colloid Science*; Oxford University Press: New York, 2001.
(9) Gradzielski, M. *Curr. Opin. Colloid Interface Sci.* **2004**, *9*, 256−263.
(10) Hofmeister, F. *Arch. Exp. Pathol. Pharmakol.* **1888**, *24*, 247−260.
(11) Zhang, Y.; Furyk, S.; Bergbreiter, D. E.; Cremer, P. S. *J. Am. Chem. Soc.* **2005**, *127*, 14505−14510.
(12) Tanford, C. *The Hydrophobic Effect: Formation of Micelles and Biological Membranes*, 2d ed; Wiley-Interscience: New York, 1980.
(13) Pratt, L. R.; Pohorille, A. *Chem. Rev.* **2002**, *102*, 2671−92.
(14) Horinek, D.; Netz, R. R. *Phys. Rev. Lett.* **2007**, *99*, 226104.
(15) Wang, L.; Friesner, R. A.; Berne, B. J. *J. Phys. Chem. B* **2010**, *114*, 7294−301.
(16) Dee, K. C. *An Introduction to Tissue-Biomaterial Interactions*; John Wiley & Sons: Hoboken, NJ, 2002; pp 1−50.
(17) Sadana, A. *Chem. Rev.* **1992**, *92*, 1799−1818.

(18) Paterová, J.; Rembert, K. B.; Heyda, J.; Kurra, Y.; Okur, H. I.; Liu, W. R.; Hilty, C.; Cremer, P. S.; Jungwirth, P. *J. Phys. Chem. B* **2013**, *117*, 8150−8158.
(19) Collins, K. D.; Neilson, G. W.; Enderby, J. E. *Biophys. Chem.* **2007**, *128*, 95−104.
(20) Collins, K. D. *Methods* **2004**, *34*, 300−311.
(21) Curtis, R. A.; Prausnitz, J. M.; Blanch, H. W. *Biotechnol. Bioeng.* **1998**, *57*, 11−21.
(22) Zhang, Y.; Cremer, P. S. *Proc. Natl. Acad. Sci. U.S.A.* **2009**, *106*, 15249−15253.
(23) Marcus, Y. *Chem. Rev.* **2009**, *109*, 1346−1370.
(24) Gurau, M. C.; Lim, S. M.; Castellana, E. T.; Albertorio, F.; Kataoka, S.; Cremer, P. S. *J. Am. Chem. Soc.* **2004**, *126*, 10522−10523.
(25) Winter, B.; Weber, R.; Schmidt, P. M.; Hertel, I. V.; Faubel, M.; Vrbka, L.; Jungwirth, P. *J Phys. Chem. B* **2004**, *108*, 14558−14564.
(26) Jungwirth, P.; Winter, B. *Annu. Rev. Phys. Chem.* **2008**, *59*, 343−366.
(27) Schwierz, N.; Horinek, D.; Netz, R. R. *Langmuir* **2013**, *29*, 2602−2614.
(28) Jubb, A. M.; Hua, W.; Allen, H. C. *Annu. Rev. Phys. Chem.* **2012**, *63*, 107−130.
(29) Mucha, M.; Frigato, T.; Levering, L. M.; Allen, H. C.; Tobias, D. J.; Dang, L. X.; Jungwirth, P. *J. Phys. Chem. B* **2005**, *109*, 7617−7623.
(30) Hopkins, A. J.; Schrödle, S.; Richmond, G. L. *Langmuir* **2010**, *26*, 10784−10790.
(31) Eftekhari-Bafrooei, A.; Borguet, E. *J. Am. Chem. Soc.* **2009**, *131*, 12034−12035.
(32) Flores, S. C.; Kherb, J.; Konelick, N.; Chen, X.; Cremer, P. S. *J. Phys. Chem. C* **2012**, *116*, 5730−5734.
(33) Chen, X.; Hua, W.; Huang, Z.; Allen, H. C. *J. Am. Chem. Soc.* **2010**, *132*, 11336−11342.
(34) Hayes, P. L.; Malin, J. N.; Konek, C. T.; Geiger, F. M. *J. Phys. Chem. A* **2008**, *112*, 660−668.
(35) Xu, M.; Tang, C. Y.; Jubb, A. M.; Chen, X.; Allen, H. C. *J. Phys. Chem. C* **2009**, *113*, 2082−2087.
(36) Zhang, Z.; Fenter, P.; Cheng, L.; Sturchio, N. C.; Bedzyk, M. J.; Predota, M.; Bandura, A.; Kubicki, J. D.; Lvov, S. N.; Cummings, P. T.; Chialvo, A. A.; Ridley, M. K.; Bénézeth, P.; Anovitz, L.; Palmer, D. A.; Machesky, M. L.; Wesolowski, D. J. *Langmuir* **2004**, *20*, 4954−4969.
(37) Luo, G.; Malkova, S.; Yoon, J.; Schultz, D. G.; Lin, B.; Meron, M.; Benjamin, I.; Vanýsek, P.; Schlossman, M. L. *Science* **2006**, *311*, 216−218.
(38) Kohli, V.; Zhang, Z.; Park, C.; Fenter, P. *Langmuir* **2010**, *26*, 950−958.
(39) Fenter, P.; Sturchio, N. C. *Prog. Surf. Sci.* **2004**, *77*, 171−258.
(40) Yan, E. C. Y.; Liu, Y.; Eisenthal, K. B. *J. Phys. Chem. B* **1998**, *102*, 6331−6336.
(41) Liu, Y.; Yan, E. C. Y.; Zhao, X.; Eisenthal, K. B. *Langmuir* **2001**, *17*, 2063−2066.
(42) Netz, R. R.; Horinek, D. *Annu. Rev. Phys. Chem.* **2012**, *63*, 401−418.
(43) Yan, E. C. Y.; Liu, Y.; Eisenthal, K. B. *J. Phys. Chem. B.* **1998**, *102*, 6331−6336.
(44) Liu, Y.; Yan, C. Y.; Zhao, X. L.; Eisenthal, K. B. *Langmuir* **2001**, *17*, 2063−2066.
(45) X Chen, X.; Z Chen, Z. *Biochim. Biophys. Acta, Biomembr.* **2006**, *1758*, 1257−1273.
(46) Huang, N.; Schlesinger, D.; Nordlund, D.; Huang, C.; Tyliszczak, T.; Weiss, T. M.; Acremann, Y.; Pettersson, L. G. M.; Nilsson, A. *J. Chem. Phys.* **2012**, *136*, 74507.
(47) Kuna, J. J.; Voitchovsky, K.; Singh, C.; Jiang, H.; Mwenifumbo, S.; Ghorai, P. K.; Stevens, M. M.; Glotzer, S. C.; Stellacci, F. *Nat. Mater.* **2009**, *8*, 837−842.
(48) Hummer, G. *Nat. Chem.* **2010**, *2*, 906−907.
(49) Garde, S.; Patel, A. J. *Proc. Natl. Acad. Sci. U.S.A.* **2011**, *108*, 16491−16492.
(50) Davis, J. G.; Gierszal, K. P.; Wang, P.; Ben-Amotz, D. *Nature* **2012**, *491*, 582−5.
(51) Godawat, R.; Jamadagni, S. N.; Garde, S. *Proc. Natl. Acad. Sci. U.S.A.* **2009**, *106*, 15119−15124.
(52) Ong, S.; Zhao, X.; Eisenthal, K. B. *Chem. Phys. Lett.* **1992**, *191*, 327−335.
(53) Wang, H.; Yan, E. C. Y.; Borguet, E.; Eisenthal, K. B. *Chem. Phys. Lett.* **1996**, *259*, 15−20.
(54) Jena, K. C.; Covert, P. A.; Hore, D. K. *J. Phys. Chem. Lett.* **2011**, *2*, 1056−1061.
(55) Eftekhari-bafrooei, A.; Borguet, E. *J. Phys. Chem. Lett.* **2011**, 1353−1358.
(56) Roy, S.; Hore, D. K. *J. Phys. Chem. C* **2012**, *116*, 22867−22877.
(57) Lambert, A. G.; Davies, P. B.; Neivandt, D. J. *Appl. Spectrosc. Rev.* **2005**, *40*, 103−145.
(58) Roke, S. *ChemPhysChem* **2009**, *10*, 1380−1388.
(59) Zhuang, X.; Miranda, P. B.; Kim, D.; Shen, Y. R. *Phys. Rev. B.* **1999**, *59*, 12632.
(60) De Beer, A. G. F.; Roke, S. *J. Chem. Phys.* **2010**, *132*, 234702.
(61) De Aguiar, H. B.; Scheu, R.; Jena, K. C.; De Beer, A. G. F.; Roke, S. *Phys. Chem. Chem. Phys.* **2012**, *14*, 6826−6832.
(62) Jena, K. C.; Scheu, R.; Roke, S. *Angew. Chem., Int. Ed.* **2012**, *51*, 12938−12940.
(63) Guyot-Sionnest, P.; Hunt, J. H.; Shen, Y. R. *Phys. Rev. Lett.* **1987**, *59*, 1597.
(64) Wang, H. F.; Gan, W.; Lu, R.; Rao, Y.; Wu, B. H. *Int. Rev. Phys. Chem.* **2005**, *24*, 191−256.
(65) Walker, R. A.; Conboy, J. C.; Richmond, G. L. *Langmuir* **1997**, *13*, 3070−3073.
(66) Vazdar, M.; Pluharová, E.; Mason, P. E.; Vácha, R.; Jungwirth, P. *J. Phys. Chem. Lett.* **2012**, *3*, 2087−2091.
(67) Schürer, B.; Wunderlich, S.; Sauerbeck, C.; Peschel, U.; Peukert, W. *Phys. Rev. B* **2010**, *82*, 241404.
(68) Tamaki, K. *Bull. Chem. Soc. Jpn.* **1967**, *40*, 38−41.
(69) Hrobárik, T.; Vrbka, L.; Jungwirth, P. *Biophys. Chem.* **2006**, *124*, 238−242.
(70) Davis, J. G.; Rankin, B. M.; Gierszal, K. P.; Ben-Amotz, D. *Nat. Chem.* **2013**, *5*, 796−802.
(71) Eschen, F.; Heyerhoff, M.; Morgner, H.; Vogt, J. *J. Phys.: Condens. Matter* **1995**, *7*, 1961.
(72) De Aguiar, H. B.; de Beer, A. G. F.; Strader, M. L.; Roke, S. *J. Am. Chem. Soc.* **2010**, *132*, 2122−2123.
(73) Vácha, R.; Roke, S. *J. Phys. Chem B.* **2012**, *116*, 11936−11942.
(74) Scheu, R.; de Aguiar, H. B.; Rankin, B. M.; Ben-Amotz, D.; Roke, S. Unpublished work 2013.
(75) Gomopoulos, N.; Lütgebaucks, C.; Sun, Q.; Macias-Romero, C.; Roke, S. *Opt. Express* **2013**, *21*, 815−821.
(76) De Aguiar, H. B.; Samson, J.-S.; Roke, S. *Chem. Phys. Lett.* **2011**, *512*, 76−80.